Supporting Information

Pantazis et al. 10.1073/pnas.0911959107

SI Materials and Methods

Data Analysis. Data were analyzed with a customized program developed in our Division. Membrane K^+ conductance (G) was calculated with the formula $G = I/(V_m - E_K)$, where I is steady-state recorded K^+ current, V_m the clamped membrane potential and E_K the equilibrium potential of K^+ with the solutions used (-62 mV). G-V and F-V curves were fitted to a Boltzmann distribution of the form: G-V= $G_{max}/(1+\exp(z(V_{half}-V_m)(F/RT))$ and F-V= $((F_{max}-F_{min})/(1+\exp(z(V_{half}-V_m)(F/RT)))-F_{min}$ where G_{max} and F_{max} are the maximum G and F, respectively; F_{min} is the minimum F; z is the effective valence; V_{half} is the half-activating membrane potential; V_m is the clamped membrane potential; F, R and T are the usual thermodynamic values. F-V curves were normalized between minimum and maximum fluorescence levels. All errors are ±1 SEM.

SI Model Description and Methodology. As in the actual BK_{Ca} channel, the model consists of four subunits, each of which contains two regulatory domains (S2 and S4) whose occupancies of resting (R) versus active (A) states depend on the activation energies $H_2 = q_2(V - V_2)$ and $H_4 = q_4(V - V_4)$, where $H_n = H_n(A) - H_n(R)$, and q_n and V_n are gating charge and half-activation voltages, respectively. A single pore unit also possesses independent voltage dependent activation with $H_P = q_P(V - V_P)$. Cooperativity arising from combined activation of two regulatory domains is described by interaction energies such as H_{4P}, and W_{24}. The opening of the pore is accompanied by a change in the global energy of jH_{4P}, where j (value: 0–4) is equal to the number of activated S4 domains. For most models, H_{2P} was set to zero (Discussion). Combined activation of S2 and S4 domains results in the addition of an interaction energy H_{24} if the two domains reside on the same subunit. W_{24} is unusual in that it is a voltage-dependent interaction term, a consequence of the excess gating charge q_{app} that arises through the proposal that mutual transition of S2 and S4 charges generates a shift in equipotential lines. Thus, $W_{24} = q_{app}(V - V_{24})$, where $V_{24} = -H_{24}/q_{app}$, and H_{24} is a voltage-independent interaction. q_{app} was set to zero for fittings of scheme II (Fig. 5 *A–J* and Fig. S1 *F–O*).

In a single subunit, the four possible configurations of S2 and S4 are as follows: RR = $\{R_2,R_4\}$, AR = $\{A_2,R_4\}$, RA = $\{R_2,A_4\}$, and AA = $\{A_2,A_4\}$. The total number of states possible in a closed-pore channel with four subunits is 30, which can be obtained by considering how many ways one can distribute four objects (subunits) among four slots (subunit configurations). For example, the state C_{1102} describes the closed state in which one subunit is in configuration RR, one is in AR, zero are in RA, and two are in AA. An additional 35 open state channels are similarly described, leading to a total number of 70 states. We employ the configurational notation C_{abcd} and O_{abcd}, where C and O are closed and open states, respectively, a is the number of subunits in configuration RR, b is the number of subunits in configuration AR, c is the number of subunits in configuration RA, d is the number of subunits in configuration AA. A valid state configuration must satisfy: $a + b + c + d = 4$.

The energies of these states are tabulated as follows: $H_{pabcd} = pH_P + b(H_2) + c(H_4 + pH_{4P}) + d(H_2 + H_4 + pH_{4P} + H_{24})$, where the pore index p is 0 or 1 depending on whether the pore is closed or open. The partition function Z of the channel is given by the following expression:

$$Z = \sum_{pabcd} \Omega_{abcd} \exp\left(\frac{-H_{pabcd}}{kT}\right),$$

where the state degeneracy $\Omega_{abcd} = 4!/a!b!c!d!$ and kT has its usual thermodynamic significance.

Computing isotherms requires evaluating the expectation value of the observable in question as a function of voltage using the following expression:

$$\langle X(V)\rangle = Z^{-1} \sum_{pabcd} X_{pabcd}\Omega_{abcd} \exp\left(\frac{-H_{pabcd}}{kT}\right).$$

The state values for normalized conductance and fluorescence change were assumed to be the following: $G_p = p$; $F2_{bd} = (b + d)/4$; and $F4_{cd} = (c + d)/4$. Inserting these expressions for X_{pabcd} in the preceding equation yields normalized isotherms that range from 0 to 1 on the voltage axis.

Model Fitting Regime. Berkeley Madonna was used to run model simulations and fit them to the data. Three "sub-models" as described above were loaded: one for pseudo-WT, one for S2-neutralized (D153Q), and one for S4-neutralized (R213G) channels. Although each submodel had its own parameter set (all listed in Fig. 5 *E*, *J*, and *O* and Fig. S1 *E* and *J*), some were fixed to be the same as the WT parameter values (marked with an asterisk in Fig. 5 and Fig. S1). Mean, normalized G-V, S2 F-V, and S4 F-V experimental datasets were loaded for WT and charge-neutralized channels, whereas the fourth-order Runge-Kutta integration algorithm was used to solve the model's differential equations and predict G-V and F-V curves according to the parameters. The three submodels were simultaneously fit, each to its respective G-V and F-V experimental dataset by using Berkeley Madonna's Curve Fitting routine with an error tolerance of 10^{-4}.

Because of the extremely shallow S2 F-V curve from S2-neutralized (D153Q) channels (lacking evident saturation within the tested membrane potential range of ±300 mV, Fig. 3*B*), the experimental data (Fig. 5 *C*, *H*, and *M* and Fig. S1*C* blue diamonds) were normalized to the prediction of the models (Fig. 5 *C*, *H*, and *M* and Fig. S1*C*, blue curve) but were not included in the simultaneous curve fitting.

Investigating Signal Cross-Talk

I. S2-S4 Signal Cross-Talk at the Macroscopic Domain. A possibility is that the fluorescence signal reported from S2 received a fractional contribution from S4 motions, and vice versa—a condition we refer to as "signal cross-talk." A consequence of this could be that neutralization of a segment would affect the TMRM fluorescence deflections observed from its intact neighbor and apparently impair their voltage dependence, without there being a functional interaction between the two segments. To investigate whether this is applicable to our data, we defined the fluorescence from S2 and S4 as the weighted sum of the underlying activation probability of S2 and S4 (P_{S2} and P_{S4}), such that:

$$\text{S4 signal} = AP_{S2} + (1 - A)P_{S4} \quad [1]$$

$$\text{S2 signal} = (1 - B)P_{S2} + BP_{S4,} \quad [2]$$

where A and B are fractional cross-talk factors between zero and one, while P_{S2} and P_{S4} are voltage-dependent segment activation probabilities, expressed as Boltzmann distributions. The free fittings of conditions **[1]** and **[2]** to the mean, normalized $\Delta F/F$

data are shown in Fig. S2, whereas the fitting parameters are shown in Table S1, below:

Table S1. Parameters for the fittings in Fig. S2

Fig. S2 plots	Clone	V_{half_S2}, mV	z_{S2}, e^0	V_{half_S4}, mV	z_{S4}, e^0	*A*	*B*
A, D	WT	−57	0.52	−83	0.78	0.066	0
B, E	D153Q	50	0.16	**−150**	**0.25**	0.13	0.20
C, F	R213G	**−140**	**0.42**	130	0.32	0.22	0.44

The best fit of the WT data demonstrates a low value for *A* and *B* ($A = 0.066$, and $B = 0$). However, because there is significant overlap between the two curves, visually acceptable fits are possible with *A* and *B* values as high as 0.5, so that an upper limit for the cross-talk variables cannot be estimated based on this fit alone. We will use additional methods to attempt to place a limit on these variables, but first a critically important point must be made regarding the hypothesis of whether cross-talk alone can explain the data, by evaluating the results for the mutant channels.

To fit the mutant data to Eq. **1** and **2**, it was absolutely necessary to change the shape of the Boltzmann curves P_{S2} and P_{S4}, even when the segment in question had not been neutralized. Therefore, although acceptable fits of the data were obtained from linear combinations P_{S2} and P_{S4} (see Table S1), this does not change the fact that neutralization of charge in one segment necessarily perturbs the voltage dependence of its neighbor (e.g., see Table S1 parameters in bold). Therefore, even with the possibility of cross-talk, the main finding of this paper, that there is mutual interaction between S2 and S4, does not change. Note that, at the same time, it does not offer a significantly better fit of the data: The sum of squared errors for single-Boltzmann fittings (which do not benefit from the six additional cross-talk parameters) is 0.0647 (cross-talk fit: 0.0490).

To reinforce the point that no degree of cross-talk can be used to avoid the conclusion of a real interaction between voltage sensors, we offer the following scenario (Fig. S3), where we constrained the fit to not allow a changes in voltage dependence of the non-neutralized segment (i.e., $P_{S2\_WT} = P_{S2\_R213G}$ and $P_{S4\_WT} = P_{S4\_D153Q}$). Under this condition, which enforces the absence of any meaningful interaction between voltage sensors, the fits are extremely poor, both visually and quantitatively (Sum Sq = 0.440), despite the fact that this condition has two additional free parameters compared to the single-Boltzmann fittings (Sum Sq = 0.0647). The fitting parameters are listed in Table S2 below.

Table S2. Fitted parameters for the constrained Boltzmann fitting described in Fig. S3

Fig. S3 plots	Clone	V_{half_S2}, mV	z_{S2}, e^0	V_{half_S4}, mV	z_{S4}, e^0	*A*	*B*
A, D	WT	−59	0.48	−97	0.67	0.30	0
B, E	D153Q	−9.3	0.17	−97*	0.67*	0.45	0.014
C, F	R213G	−59*	0.48*	79	0.21	0	0.45

Parameters of mutant channels marked with an asterisk (*) were constrained to be equal to their wild-type equivalent.

Investigating cross-talk at the macroscopic domain demonstrates that signal cross-talk alone (without S2–S4 interaction) cannot account for the observed experimental data. However, the fitting of Boltzmann distributions provides very little mechanistic information and it oversimplifies the underlying complexities of a microscopic model. To better understand whether cross-talk is sufficient to account for the apparent interactions between S2 and S4, we implemented cross-talk factors in our allosteric model framework, as follows.

II. S2–S4 Signal Cross-Talk at the Microscopic Level. In Fig. S4 *A–D*, we globally fit the data with a variant of our allosteric model in which S2 and S4 activation are not linked by energetic, mechanical, or any other kind of interaction, although S4 is still allosterically linked to the pore domain. The cross-talk mechanism was implemented as follows: Activation of a segment produces a change in its fluorescence, represented by values $F_{2\leftarrow S2}$ and $F_{4\leftarrow S4}$ for S2 and S4 signal, respectively. These values were fixed to 1. In addition, activation of S2 induces a fractional change in the fluorescence of the S4 signal (value $F_{4\leftarrow S2}$). Likewise, activation of S4 perturbs S2 fluorescence signal by the term $F_{2\leftarrow S4}$. The cross-talk terms $F_{4\leftarrow S2}$ and $F_{2\leftarrow S4}$ were fit freely for each BK_{Ca} channel clone.

These microscopic terms can be roughly related to the macroscopic variables (*A* and *B*) through the relations: $A = F_{4\leftarrow S2}/(F_{4\leftarrow S2} + F_{4\leftarrow S4})$, and $B = F_{2\leftarrow S4}/(F_{2\leftarrow S4} + F_{2\leftarrow S2})$.

The fits are visibly poor, demonstrating that cross-talk alone cannot account for the data. This is in agreement with the analogous macroscopic Boltzmann fittings (Fig. S3). As an aside, inclusion of an S2-Pore interaction (H_{2P}) did not improve the goodness of the fit.

Finally, to estimate a reasonable value for an upper limit of the cross-talk values, we attempted to improve the fits of the dynamic field and mechanical interaction models used in the main paper by adding $F_{2\leftarrow S4}$ and $F_{4\leftarrow S2}$ to the fitted variables. The inclusion of cross-talk in the mechanical interaction model (Fig. 5 *F–J*, scheme III) is included in Fig. S4 *E–H*, whereas the same for the dynamic field focusing model (Fig. 5 *K–O*, scheme IV) is included in Fig. S4 *I–L*. For an easier comparison between models with and without cross-talk, please see Tables S3 and S4 below

Table S3. Mechanical interaction or nudging mechanism (Scheme III)

	Zero cross-talk (Fig. 5 *F–J*)				With cross-talk (Fig. S4 *E–H*)			
Parameter:	*A*	*B*	α	β	*A*	*B*	α	β
WT channels	0	0	0.21	0.45	0.18	0.0076	0.28	0.46
D153Q (S2 neutralized)	0	0	0.21*	0.45*	0.039	2.1×10^{-6}	0.28*	0.46*
R213G (S4 neutralized)	0	0	0.21*	0.45*	0	0.16	0.28*	0.46*

Parameters of mutant channels marked with an asterisk (*) were constrained to be equal to their wild-type equivalent.

Table S4. Dynamic field focusing mechanism (Scheme IV)

	Zero cross-talk (Fig. 5 *K–O*)			With cross-talk (Fig. S4 *I–L*)		
Parameter:	*A*	*B*	q_{app}, e^0	*A*	*B*	q_{app} (e^0)
WT channels	0	0	0.21	2.2×10^{-8}	0.0076	0.24
D153Q (S2 neutralized)	0	0	0.0063	0.058	0	1.8×10^{-6}
R213G (S4 neutralized)	0	0	0.0027	0.0065	1.8×10^{-7}	0.0058

Where *A* and *B* are defined in terms of the microscopic cross-talk variables as above, α and β are the fractions of S2 and S4 nudged during activation according to the interpretation of scheme III and q_{app} is the apparent additional charge caused by field focusing (scheme IV). The fitted values of *A* and *B* represent a reasonable upper limit of cross-talk in the context of two possible models that explain our data. In no case do they exceed

20% of the observed signal. It should also be noted that fits did not improve markedly, and the model-specific parameters (α, β, q_{app}) did not change substantially—if anything, there appears to be a slightly greater extent of mechanical interaction or field focusing.

In conclusion, the introduction of cross-talk factors does not relieve the necessity of some type of mutual interaction between S2 and S4 as a means of explaining our data. If cross-talk does occur, it is likely a minor effect, as estimated by only limited improvements in our ability to fit data with reasonable models.

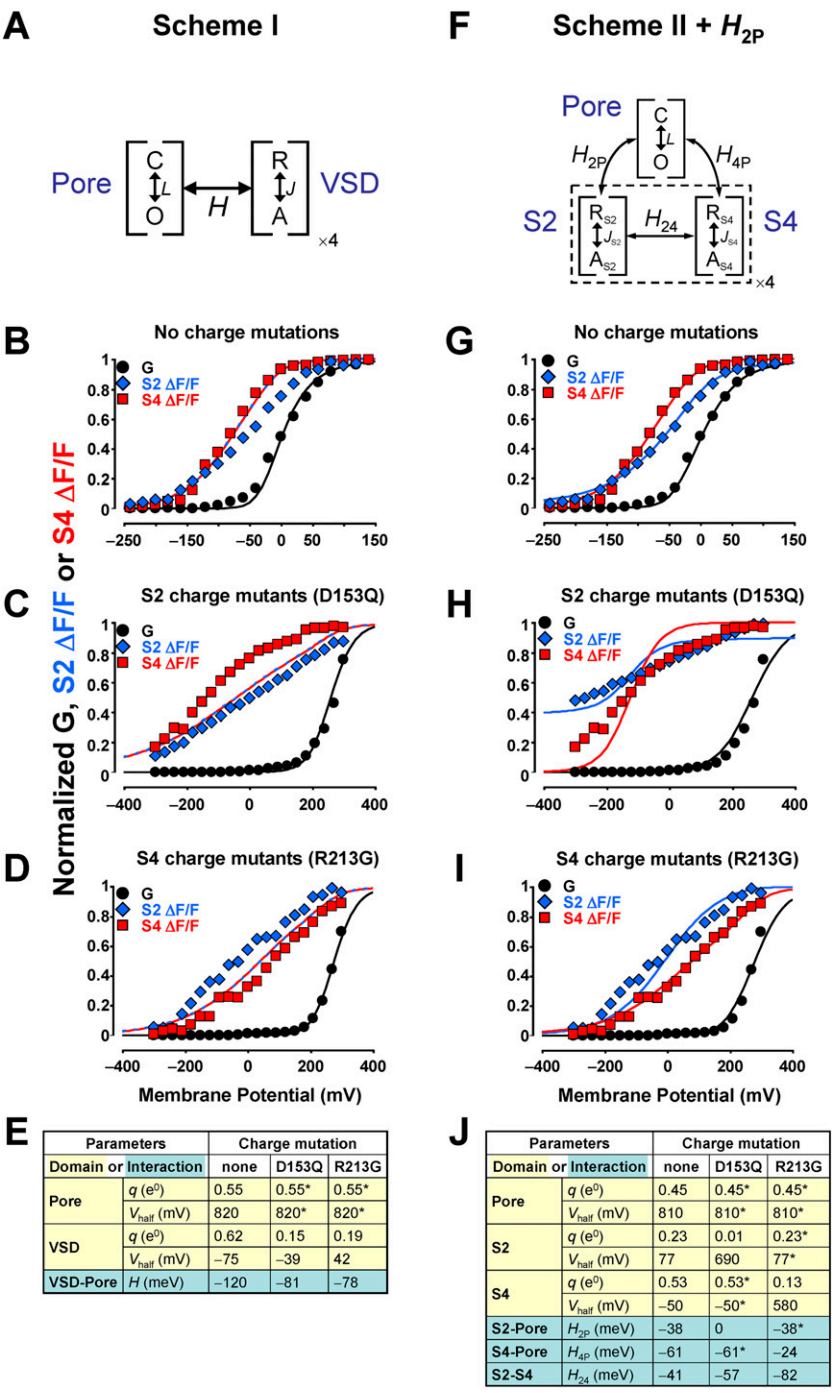

E

Parameters		Charge mutation		
Domain or Interaction		none	D153Q	R213G
Pore	q (e^0)	0.55	0.55*	0.55*
	V_{half} (mV)	820	820*	820*
VSD	q (e^0)	0.62	0.15	0.19
	V_{half} (mV)	–75	–39	42
VSD-Pore	H (meV)	–120	–81	–78

J

Parameters		Charge mutation		
Domain or Interaction		none	D153Q	R213G
Pore	q (e^0)	0.45	0.45*	0.45*
	V_{half} (mV)	810	810*	810*
S2	q (e^0)	0.23	0.01	0.23*
	V_{half} (mV)	77	690	77*
S4	q (e^0)	0.53	0.53*	0.13
	V_{half} (mV)	–50	–50*	580
S2-Pore	H_{2P} (meV)	–38	0	–38*
S4-Pore	H_{4P} (meV)	–61	–61*	–24
S2-S4	H_{24} (meV)	–41	–57	–82

Fig. S1. Alternative models. (*A*) Scheme I: the BK_{Ca} VSD is a superunit with uniform voltage dependence, so the activations of S2 and S4 are indistinguishable. The Pore domain can assume the closed (C) or open (O) state, whereas each VSD (from each α subunit) can be either resting (R) or active (A). VSD activation stabilizes Pore opening via interaction *H*. (*B*) Normalized K^+ conductance (G, black circles), S2 Δ*F*/*F* (blue diamonds) and S4 ΔF/F (red squares) from channels without charge neutralization (Fig. 2). Scheme I predictions for conductance and VSD activation are shown as black and blue/red curves, respectively. (*C*) As in *B* for channels with mutation D153Q in S2 (Figs. 3 *A*–*C* and 4 *D*–*F*). (*D*) As in *B*, for channels with mutation R213G in S4 (Figs. 3 *D*–*F* and 4 *A*–*C*). (*E*) Scheme I fitted parameters. Parameters of charge-neutralized channels with an asterisk were constrained to be equal to their pseudo-WT channel equivalent. (*F*) Scheme II (Fig. 5*A*) with the addition of an S2-Pore interaction H_{2P}. (*G*–*J*) As in *B*–*E*, for scheme II + H_{2P}. Model predictions of S2 and S4 activations are blue and red curves, respectively. In *H*, the highly linear S2 Δ*F*/*F* data (blue diamonds; also see Fig. 3*B*) were renormalized to conform to the model prediction (blue curve), instead of constraining it.

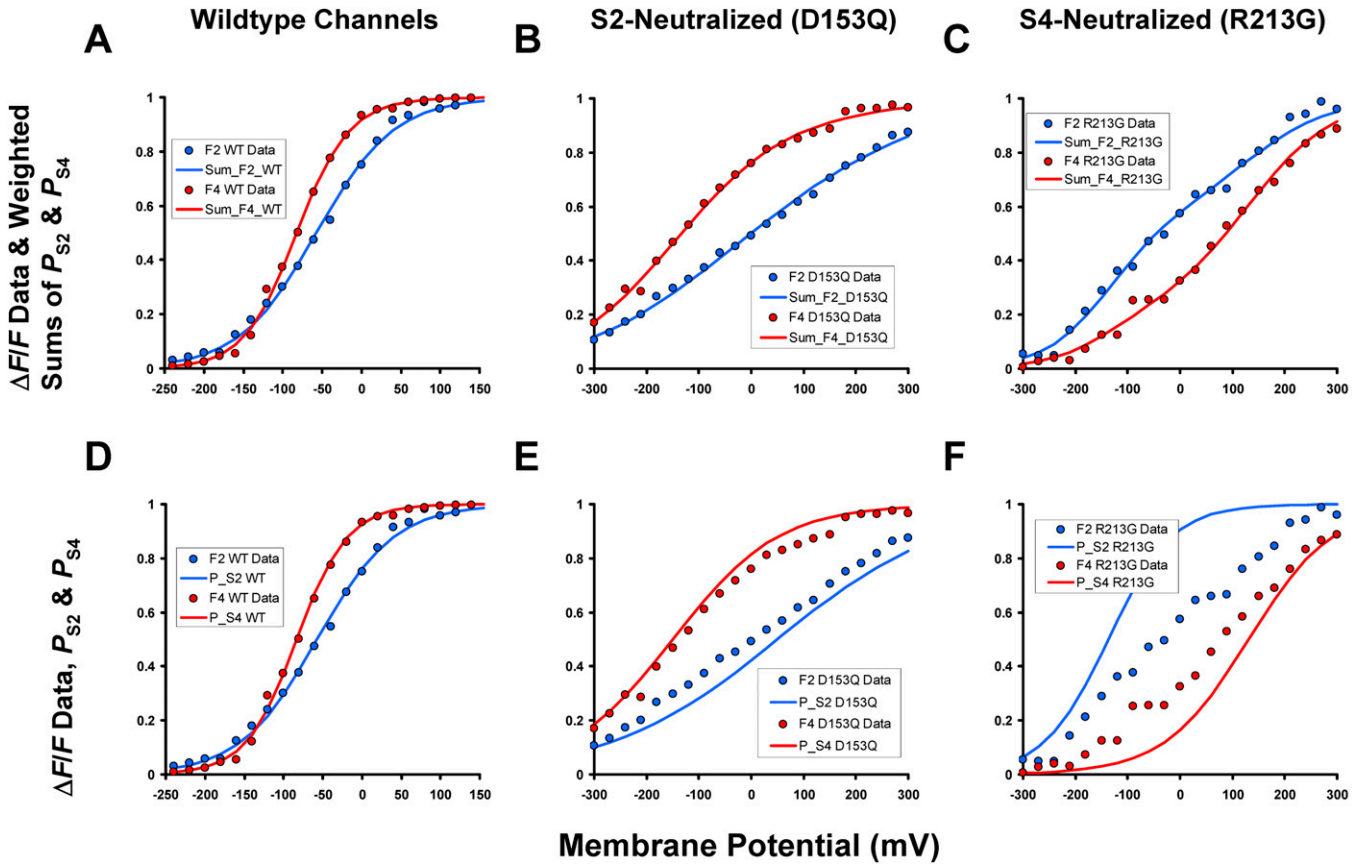

Fig. S2. Cross-talk at the macroscopic domain I: Free parameter fitting. (*A–C*) To investigate the possibility of cross-talk accounting for the experimental data, the normalized, mean Δ*F/F* data from S2 (blue circles) and S4 (red circles) from channels without charge neutralization mutation (*A*), channels with a neutralized voltage-sensing charge in S2 (D153Q, *B*), and channels with a neutralized S4 (R213G, *C*) were fitted with the weighted sums (linear combinations) of two Boltzmann distributions (P_{S2} and P_{S4}), reflecting the underlying voltage dependence of S2 and S4 activation, respectively. The blue and red curves represent these weighted sums fit to S2 and S4 fluorescence data, respectively. The cumulative sum of squared errors is 0.0490. The fitting parameters are listed in Table S1 and discussed in *SI Text*, "Investigating Signal Cross-Talk." (*D–F*) Fluorescence data are shown as in *A–C* for the corresponding BK_{Ca} clones used. Instead of the weighted sums, the individual constituent Boltzmann distributions (P_{S2} and P_{S4}) are shown as blue and red curves, respectively.

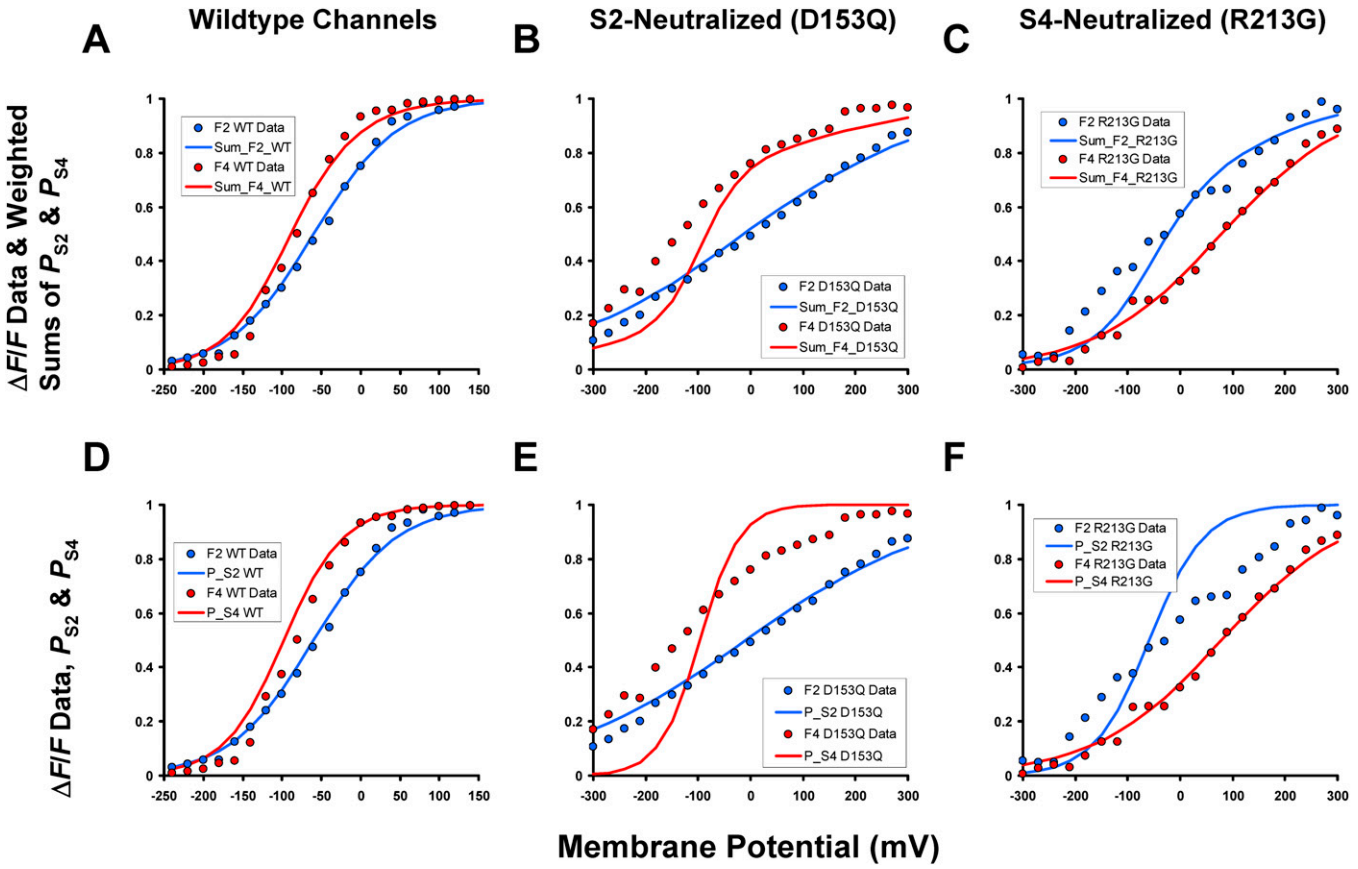

Fig. S3. Cross-talk at the macroscopic domain II: Cross-talk cannot exclude S2–S4 interactions. The data and curves shown are as in Fig. S2. In these fits, interactions between S2 and S4 are excluded, by introducing the constraint that the voltage dependence of segment activation is not perturbed by charge neutralization in the opposite segment. In this case, $P_{S2\_WT} = P_{S2\_R213G}$ and $P_{S4\_WT} = P_{S4\_D153Q}$. The cumulative sum of squared errors is 0.440. The fitting parameters are listed in Table S2 and discussed in *SI Text*, "Investigating Signal Cross-Talk," section I.

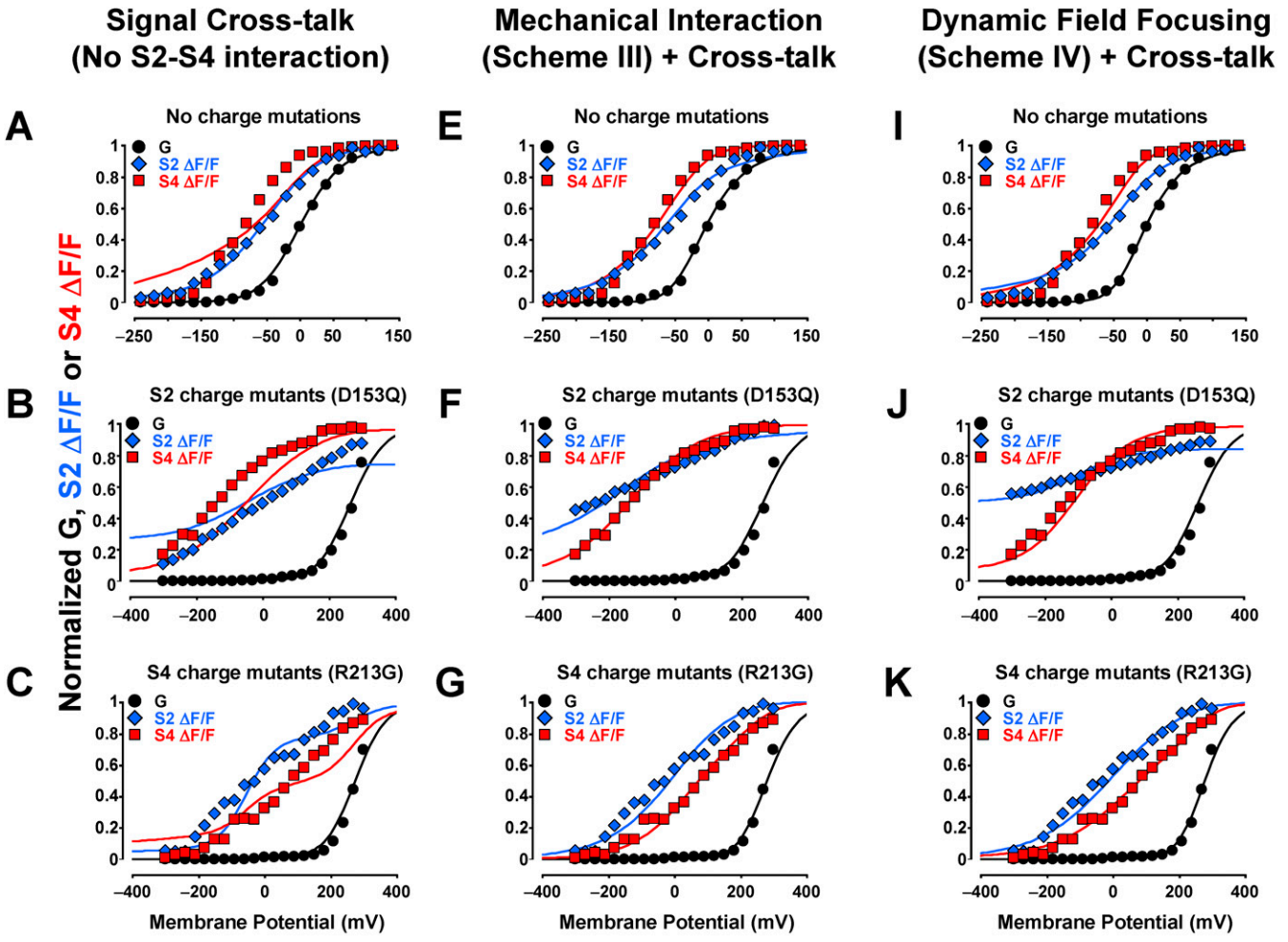

D

Parameters		Charge mutation		
Domain or Interaction		none	D153Q	R213G
Pore	q (e^0)	0.45	0.45*	0.45*
	V_{half} (mV)	800	800*	800*
S2	q (e^0)	0.60	0	0.60*
	V_{half} (mV)	−53	0	−53*
S4	q (e^0)	0.24	0.24*	0.042
	V_{half} (mV)	−47	−47*	620
S4-Pore	H_{4P} (meV)	−100	−61	−84
Cross-talk	$F_{2\leftarrow S4}$	0.25	0.93	0.47
	$F_{4\leftarrow S2}$	0	0.084	0.37

H

Parameters		Charge mutation		
Domain or Interaction		none	D153Q	R213G
Pore	q (e^0)	0.47	0.47*	0.47*
	V_{half} (mV)	800	800*	800*
S2	q (e^0)	0.32	0	0.32*
	V_{half} (mV)	93	320	93*
S4	q (e^0)	0.28	0.28*	0.044
	V_{half} (mV)	13	13*	620
S4-Pore	H_{4P} (meV)	−100	−63	−65
S2-S4	H_{24} (meV)	−62	−47	−94
	α	0.28	0.28*	0.28*
	β	0.46	0.46*	0.46*
Cross-talk	$F_{2\leftarrow S4}$	0.22	0	2.1×10^{-6}
	$F_{4\leftarrow S2}$	0.0075	0.041	0.19

L

Parameters		Charge mutation		
Domain or Interaction		none	D153Q	R213G
Pore	q (e^0)	0.49	0.49*	0.49*
	V_{half} (mV)	820	820*	820*
S2	q (e^0)	0.18	0	0.18*
	V_{half} (mV)	98	320	98*
S4	q (e^0)	0.32	0.32*	0.11
	V_{half} (mV)	14	14*	590
S4-Pore	H_{4P} (meV)	−100	−68	−71
S2-S4	H_{24} (meV)	−57	−42	−73
	q_{app} (e^0)	0.24	0	0.01
Cross-talk	$F_{2\leftarrow S4}$	0.0077	0	1.8×10^{-7}
	$F_{4\leftarrow S2}$	2.2×10^{-8}	0.062	0.0066

Fig. S4. Investigating cross-talk at the microscopic level. (*A–D*) Fitting of a statistical-mechanical model (as in Fig. 5 and Fig. S1) without any interaction between S2 and S4. Instead, activation of S4 contributes to the fluorescent signal from S2, as expressed by cross-talk term $F_{2\leftarrow S4}$. Likewise, S2 activation contributes to S4 fluorescence by factor $F_{4\leftarrow S2}$. (*A*) Normalized mean K^+ conductance (G, black circles), S2 Δ*F*/*F* (blue diamonds) and S4 Δ*F*/*F* (red squares) from channels without charge neutralization ("pseudo-WT", Fig. 2). Predictions of this model for conductance and S2 and S4 fluorescence signals are shown as black, blue, and red curves, respectively. (*B*) As in *A*, for channels with a charge neutralization mutation in S2 (D153Q). (*C*) As in *A*, for channels with a charge neutralization mutation in S4 (R213G). (*D*) The fitting parameters of the model. Parameters of charge-neutralized channels with an asterisk were constrained to be equal to their pseudo-WT channel equivalent. (*E–H*) As in *A–D*. This time, a model similar to scheme III (Fig. 5*F*) was fit, with the addition of signal cross-talk parameters $F_{S2\leftarrow S4}$ and $F_{S4\leftarrow S2}$. In *F*, the highly-linear S2 Δ*F*/*F* data (blue diamonds; also see Fig. 3*B*) were renormalized to conform to the model prediction (blue curve), instead of constraining it. (*I–L*) As in *E–H*. This time, a model similar to scheme IV (Fig. 5*K*) was fit, including cross-talk parameters $F_{S2\leftarrow S4}$ and $F_{S4\leftarrow S2}$. See *SI Text*, "Investigating Signal Cross-Talk," section II, for a discussion of the fittings.

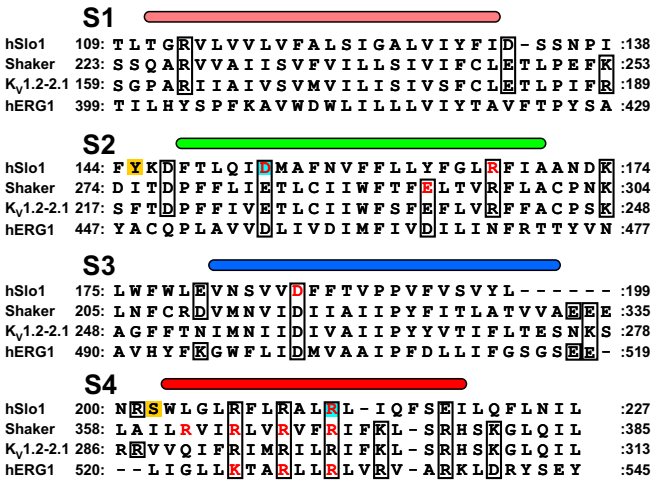

Fig. S5. Voltage sensor domain homology. Alignment of the VSDs of *hSlo1*, encoding the human BK_{Ca} a subunit; *Shaker*, encoding a *Drosophila* voltage-gated K^+ channel; the human *Ether-à-go-go related gene*, encoding HERG; and the K_V1.2-2.1 chimera, used to produce the most recent crystal structure of a VSD to date (1). Positions of the transmembrane domains S1-S4 are shown (colored bars) as resolved from K_V1.2-2.1. Conserved charged residues are boxed. Voltage-sensing residues in BK_{Ca} (2), *Shaker* (3,4) and HERG (5) channels are in red type. BK_{Ca} residues substituted to cysteine for TMRM labeling are highlighted in orange; neutralized voltage-sensing residues in blue.

1. Long SB, Tao X, Campbell EB, MacKinnon R (2007) Atomic structure of a voltagedependent K+ channel in a lipid membrane-like environment. *Nature* 450:376–382.
2. Ma Z, Lou XJ, Horrigan FT (2006) Role of charged residues in the S1-S4 voltage sensor of BK channels. *J Gen Physiol* 127:309–328.
3. Seoh SA, Sigg D, Papazian DM, Bezanilla F (1996) Voltage-sensing residues in the S2 and S4 segments of the Shaker K+ channel. *Neuron* 16:1159–1167.
4. Aggarwal SK, MacKinnon R (1996) Contribution of the S4 segment to gating charge in the Shaker K+ channel. *Neuron* 16:1169–1177.
5. Zhang M, Liu J, Tseng GN (2004) Gating charges in the activation and inactivation processes of the HERG channel. *J Gen Physiol* 124:703–718.

.